Sriram Sridharan[1]
Junjie Zhu[1]
Guoqing Hu[2]
Xiangchun Xuan[1]

[1]Department of Mechanical Engineering, Clemson University, Clemson, SC, USA
[2]LNM, Institute of Mechanics, Chinese Academy of Sciences, Beijing, P. R. China

Received January 5, 2011
Revised March 27, 2011
Accepted April 1, 2011

Research Article

Joule heating effects on electroosmotic flow in insulator-based dielectrophoresis

Insulator-based dielectrophoresis (iDEP) is an emerging technology that has been successfully used to manipulate a variety of particles in microfluidic devices. However, due to the locally amplified electric field around the in-channel insulator, Joule heating often becomes an unavoidable issue that may disturb the electroosmotic flow and affect the particle motion. This work presents the first experimental study of Joule heating effects on electroosmotic flow in a typical iDEP device, e.g. a constriction microchannel, under DC-biased AC voltages. A numerical model is also developed to simulate the observed flow pattern by solving the coupled electric, energy, and fluid equations in a simplified two-dimensional geometry. It is observed that depending on the magnitude of the DC voltage, a pair of counter-rotating fluid circulations can occur at either the downstream end alone or each end of the channel constriction. Moreover, the pair at the downstream end appears larger in size than that at the upstream end due to DC electroosmotic flow. These fluid circulations, which are reasonably simulated by the numerical model, form as a result of the action of the electric field on Joule heating-induced fluid inhomogeneities in the constriction region.

Keywords:
Electroosmotic flow / Electrothermal flow / Insulator-based dielectrophoresis / Joule heating / Microfluidics
DOI 10.1002/elps.201100011

1 Introduction

As a versatile tool, dielectrophoresis (DEP) has been widely used to focus, trap, concentrate and separate cells, viruses, and biomolecules in microfluidic devices for various lab-on-a-chip applications [1–3]. DEP refers to the induced motion of particles (either charged or non-charged) in a non-uniform electric field [4]. The electric field gradients in these devices are created by either microelectrodes [5, 6] or micro insulators [7–9]. In electrode-based dielectrophoresis (eDEP), pairs of microelectrodes are placed inside a microchannel. High-frequency AC voltages are supplied to achieve strong electric fields/gradients and suppress electrochemical reactions on electrode surfaces [10–17]. In insulator-based dielectrophoresis (iDEP), both DC and AC voltages (of any frequency) can be applied to the remote electrodes positioned in end-channel reservoirs for transporting and manipulating particles. The electric field gradients are caused by the blockage of electric current due to in-channel hurdles, posts, and ridges [18–27].

Both eDEP and iDEP devices may potentially suffer from the issue of Joule heating in the suspending medium due to the locally amplified electric field around micro electrodes or insulators (typically on the order of hundreds of kV/m) [28, 29]. It has been long known in capillary electrophoresis that Joule heating can elevate the buffer temperature and disturb the electroosmotic flow causing significant sample dispersion [30–33]. The effects of Joule heating on fluid temperature and motion in eDEP have been investigated previously [34–38]. It was reported that a pair of counter-rotating fluid circulations could form near the microelectrodes [39]. This so-called electrothermal flow is a consequence of the interactions between the applied AC electric field and the Joule heating-induced gradients of fluid conductivity and permittivity [40, 41]. Its magnitude is proportional to the fourth power of the local electric field. Electrothermal fluid circulations can also take place in AC electrowetting when the frequency of the applied electric field is much greater than the typical frequency of electrode polarization [42, 43]. Recently, electrothermal flow has been demonstrated to enhance microfluidic mixing [44] and immunoassays [45] and to pump biofluids [46, 47] as well.

Correspondence: Professor Xiangchun Xuan, Department of Mechanical Engineering, Clemson University, Clemson, SC 29634-0921, USA
E-mail: xcxuan@clemson.edu
Fax: +1-864-656-7299

Abbreviations: eDEP, electrode-based dielectrophoresis; **iDEP,** insulator-based dielectrophoresis; **PDMS,** poly (dimethylsiloxane)

Colour Online: See the article online to view Figs. 1, 3, 4, 5 in colour.

To date, however, very little work has been performed on Joule heating and its effects on electroosmotic flow in iDEP devices. Sabounchi et al. [48] characterized their iDEP polymeric devices using thermometry experiments and numerical modeling. They observed that Joule heating creates an asymmetric temperature distribution that disturbs the distribution of electric field and electrokinetic forces. Very recently, Hawkins and Kirby [49] developed a numerical model to simulate the electrothermal flow in a two-dimensional constriction in channel depth under DC-offset AC electric fields. They found that fluid circulations may occur in the constriction region at appropriate conditions. It was also predicted that the electrothermal flow effects serve to enhance dielectrophoretic particle deflection and trapping in almost all cases. In this work, we provide the first experimental demonstration of electrothermal flow circulations in iDEP devices that are best represented by a constriction microchannel. We also perform a numerical modeling of the coupled electric, heat and fluid transport phenomena in order to understand the process and simulate the observed electroosmotic flow patterns in the experiment.

2 Materials and methods

2.1 Experiment

The microchannel was fabricated in poly(dimethylsiloxane) (PDMS) using the standard soft lithography technique. It was bonded to a regular glass slide after air plasma treating (PDC-32G, Harrick Scientific, Ossining, NY). The detailed procedure is provided in Ref. [25]. As shown in Fig. 1, the channel is 1 cm long with a 200 μm-length constriction in the middle. The widths of the channel and constriction are 400 and 40 μm, respectively. The channel is uniformly 40 μm deep. The electric field was supplied by a function generator (33220A, Agilent Technologies, Santa Clara, CA) in conjunction with a high-voltage amplifier (609E-6, Trek, Medina, NY). Fluorescent polystyrene microspheres of 590 nm in diameter (Bangs Laboratories, USA) were used to visualize the flow pattern. They were suspended in 5 mM phosphate buffer with a measured electric conductivity of 470 μS/m at room temperature. Particle motion was monitored using an inverted microscope (Nikon Eclipse TE2000U, Nikon Instruments, Lewisville, TX), through which videos and images were recorded using a CCD camera (Nikon DS-Qi1Mc). The captured digital videos and images were processed using the Nikon imaging software (NIS-Elements AR 2.30). Pressure-driven flow was eliminated by carefully balancing the liquid heights in the two reservoirs prior to every experiment.

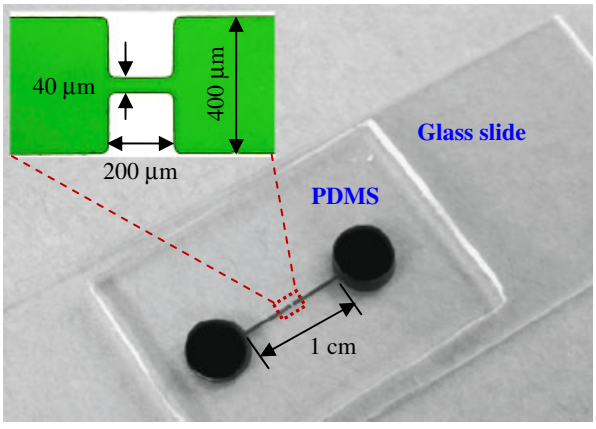

Figure 1. Picture of the constriction microchannel with dimensions labeled in the inset.

2.2 Theory

This section first presents the governing equations for the coupled electric, heat and fluid transport phenomena that typically take place in iDEP devices. Next, the computational domain is described for the constriction microchannel under investigation. The necessary boundary conditions for solving the governing equations in this domain are then summarized. Finally, the numerical method is presented along with the material properties that are needed in the modeling.

2.2.1 Governing equations

2.2.1.1 Electric field

With the assumption of non-conducting PDMS and glass substrates, the applied electric field, $\mathbf{E}$, is confined within the fluid and is governed by the following two equations [40]:

$$\nabla \cdot (\varepsilon \mathbf{E}) = \rho_e \tag{1}$$

$$\nabla \cdot (\sigma \mathbf{E}) + \frac{\partial \rho_e}{\partial t} = 0 \tag{2}$$

where ε is the permittivity of the fluid, ρ_e is the free charge density, σ is the electrical conductivity of the fluid, and t is the time coordinate. Note that the convection current has been assumed negligible as compared with the conduction current, $\sigma\mathbf{E}$, in Eq. (2). Combining Eqs. (1) and (2) gives rise to a quasi-electrostatic equation for the electric potential [40], ϕ

$$\nabla \cdot [(\sigma + i\omega\varepsilon)\nabla\phi] = 0 \tag{3}$$

where $\omega = 2\pi f$ is the angular frequency of the electric field with f being the ordinary frequency, and $\mathbf{E} = -\nabla\phi$. It is important to note that Eq. (3) is only applicable to a sinusoidally varying potential with a single frequency. For DC fields and AC fields with $f \ll \sigma/2\pi\varepsilon$ (typically on the order of MHz [35, 37, 41]), Eq. (3) reduces to

$$\nabla \cdot (\sigma \nabla\phi) = 0 \tag{4}$$

which is the case in this work.

2.2.1.2 Temperature field

The application of electric field induces Joule heating within the fluid, which, however, extends to both the PDMS and

the glass substrates through thermal diffusion in all three dimensions [50]. This significantly complicates the thermal modeling. We therefore restrict our thermal analysis to the fluid phase, and moreover, consider only the heat conduction and convection in the horizontal plane. The real three-dimensional heat transfer conditions surrounding the fluid are approximately simulated by a uniform heat conduction boundary condition normal to the channel wall. We find that this simplified 2D model is sufficient to capture the main feature of electroosmotic flow that was observed in our experiments as demonstrated in Section 4. The steady time-averaged temperature field, T, in the fluid is governed by the following energy equation:

$$\rho C_p(\mathbf{u}\cdot\nabla T) = \nabla\cdot(k\nabla T)+\sigma\langle\mathbf{E}^2\rangle \quad (5)$$

where ρ is the fluid density, C_p is the specific heat capacity of the fluid, $\mathbf{u}$ is the fluid velocity, k is the thermal conductivity of the fluid, and the last term represents the time-averaged Joule heating. Note that the convective term on the left-hand side of Eq. (5) may not be neglected because the thermal Peclet number (i.e. the ratio of the rate of heat convection to that of heat diffusion) can easily reach the order of 1 in our experiments.

2.2.1.3 Flow field

The steady-state flow field of the fluid is governed by the Navier–Stokes equation along with the continuity equation [40],

$$\rho\mathbf{u}\cdot\nabla\mathbf{u} = -\nabla p+\nabla\cdot(\eta\nabla\mathbf{u})+\langle\mathbf{f}_e\rangle \quad (6)$$

$$\nabla\cdot\mathbf{u} = 0 \quad (7)$$

where p is the pressure, η is the dynamic viscosity of the fluid, and $\langle\mathbf{f}_e\rangle$ is the time-averaged electrical body force or the so-called electrothermal force [40]. The general form of $\langle\mathbf{f}_e\rangle$ is given as [51]

$$\langle\mathbf{f}_e\rangle = \langle\rho_e\mathbf{E}-0.5\mathbf{E}^2\nabla\varepsilon\rangle \quad (8)$$

where the first and second terms on the right-hand side represent the Coulomb force and dielectric force, respectively. Replacing the free charge density, ρ_e, with Eq. (1) rewrites Eq. (8) as

$$\langle\mathbf{f}_e\rangle = \langle(\varepsilon\nabla\cdot\mathbf{E}+\alpha\varepsilon_0\mathbf{E}\cdot\nabla T)\mathbf{E}-0.5\alpha\varepsilon_0\mathbf{E}^2\nabla T\rangle \quad (9)$$

where α is the linear temperature coefficient of fluid permittivity, i.e. $\varepsilon/\varepsilon_0 = 1+\alpha(T-T_0)$ with ε_0 being the fluid permittivity at the reference temperature T_0. Therefore, it is the interaction of electric field with Joule heating-induced temperature gradients that generate the volume electrothermal force.

2.2.2 Computational domain and boundary conditions

As noted earlier, we consider only the fluid phase in the numerical model and solve for the coupled electric potential, temperature, and flow fields in two dimension for simplicity.

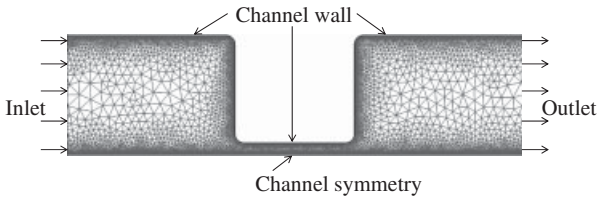

Figure 2. Zoom-in top view of the meshed constriction region of the microchannel. Note that the computational domain comprises one half of the entire microchannel (i.e. 1 cm by 200 μm).

Due to the symmetry with respect to the channel centerline, the computational domain comprises one half of the entire microchannel in the horizontal plane (i.e. 1 cm by 200 μm). Figure 2 shows the close-up view of the meshed constriction region (meshing parameters will be explained later in Section 3.3). To solve for the coupled electric, energy, and fluid equations (4)–(7), four sets of boundary conditions are imposed to the inlet, outlet, channel wall, and channel symmetry as highlighted in Fig. 2. These boundary conditions (except the symmetric ones) are summarized below.

2.2.2.1 Electric field

Inlet: $\phi = V_0$, where V_0 is the applied electric potential.

Outlet: $\phi = 0$, i.e. grounded.

Channel wall: $\mathbf{n}\cdot(\sigma\nabla\phi) = 0$, i.e. electrically insulating, where $\mathbf{n}$ denotes the unit normal vector.

2.2.2.2 Temperature field

Inlet and outlet: $T = T_0$, i.e. the fluids in the end-channel reservoirs are assumed isothermal as their volumes are much larger than the fluid within the microchannel [49, 53].

Channel wall: $q'' = -h(T-T_0)$, where q'' is the outward heat flux due to conduction with an assumed heat transfer coefficient h. The magnitude of h is determined by matching the model predicted rise in electric current with the experimentally measured data. This value is assumed constant throughout the channel wall and independent of the fluid temperature for simplicity.

2.2.2.3 Flow field

Inlet and outlet: $\mathbf{n}\cdot(\eta\nabla\mathbf{u}) = 0$ and $p = 0$, i.e. the fluids in the end-channel reservoirs are assumed to have zero viscous stress and zero pressure (open to the air).

Channel wall: $\mathbf{u} = \varepsilon\zeta\nabla\phi_{DC}/\eta$, where ζ is the zeta potential of the channel wall. This is a well-accepted slip boundary condition for electroosmotic flow in microchannels with thin electric double layers (approximately 5 nm for the buffer solution used in this work) [52]. It is important to note that only the DC component of the applied voltage drop, ϕ_{DC}, can drive electroosmotic flow. However, both the DC and AC components generate Joule heating and contribute to electrothermal flow via the

electrothermal force, ($\mathbf{f}_e$) in Eq. (6). This indicates that we can vary the relative strength of electroosmotic flow and electrothermal flow by adjusting the DC to AC field ratio, which will be demonstrated in Section 4.

2.2.3 Numerical method and material properties

Numerical simulation was carried out using the COMSOL 3.5a multiphysics software (Burlington, MA). The Conductive Media DC, Convection and Conduction, and Incompressible Navier–Stokes modules were used to solve for the coupled electric potential, temperature, and flow fields. The Convection and Conduction module was chosen from the COMSOL Multiphysics application mode. The Conductive Media DC and Incompressible Navier–Stokes modules were selected from the MEMS application mode. The 2D geometry of one half of the entire microchannel was created using the drawing tools in COMSOL. The geometry was then meshed with triangular meshes using the free mesh parameters tool box. The boundaries are more densely meshed with the maximum element size of 5 μm, and the whole domain contains a total of around 100 000 elements. The constriction region consists of more mesh elements than the rest of the channel. Model validation was performed by increasing the number of mesh elements ranging from 5000 to 200 000. There was no noticeable change in the results when the number of mesh elements was beyond 50 000. In addition, as COMSOL can only handle pure DC or pure AC electric fields, we have to modify the governing equations (4)–(7) to accommodate DC-biased AC electric fields that were used in our experiment. The details are provided in the appendix (Section 6).

Temperature is the coupling parameter in solving the electrical, energy and fluid equations as it affects the fluid properties. We considered the temperature dependence of fluid permittivity, electric conductivity and viscosity using the following expressions [31]:

$$\varepsilon(T) = \varepsilon_0[1+\alpha(T - T_0)] \tag{10}$$

$$\sigma(T) = \sigma_0[1+\beta(T - T_0)] \tag{11}$$

$$\eta(T) = 2.761 \times 10^{-6} \exp(1713/T) \tag{12}$$

where σ_0 is the electric conductivity of the fluid at the reference temperature, and β is its linear temperature coefficient. The values of the constants and fluid properties involved in the numerical simulation are listed in Table 1.

The convective heat transfer coefficient, h, was determined by matching the model predicted rise in electric current density with the experimentally measured increase in electric current. In our experiment the electric current increased from the initial 52 μA (at the room temperature) to a quasi-steady 66 μA three minutes after a 600 V voltage drop (either DC or AC RMS) was applied across the constriction microchannel. In COMSOL, an initial value of h was first assumed to start the 2D simulation. The electric current density was read directly from the predefined quantity in COMSOL, total current density, at a position that was near the outlet of the microchannel. Its rise due to Joule heating was determined by comparing the electric current densities at the same position of the microchannel when Joule heating is absent and present, respectively. Thus, the obtained value was then compared with the experimentally measured increase in electric current (which is about 27%). If these values did not match, a new value of h was assigned to repeat the above steps.

Table 1. Summary of the constants and fluid properties used in the model [54]

Name	Value	Unit	Description
T_0	293	K	Reference temperature
ε_0	7.10×10^{-10}	F/m	Fluid permittivity at T_0
α	−0.0046	1/K	Temperature coefficient of fluid permittivity
σ_0	0.047	S/m	Fluid electric conductivity at T_0
β	0.02	1/K	Temperature coefficient of fluid electric conductivity
ρ	1000	kg/m^3	Fluid density
C_p	4.186	kJ/(kg K)	Fluid heat capacity
K	0.6	W/(m K)	Fluid thermal conductivity
ζ	−0.05	V	Wall ζ potential
H	20×10^3	W/(m^2 K)	Convective heat transfer coefficient

Using this iteration method, we found that the assumption of $h = 20 \times 10^3$ W/(m^2 K) (see Table 1) in our 2D model yielded the closest match with the experimental data. This h value is recognized to be much larger than that reported in Ref. [49] and those used in other studies [50, 56, 57], which indicate that Joule heating of the fluid was dissipated mainly through the bottom glass slide in our microchannel. It is because glass has a much higher thermal conductivity than PDMS [50, 56, 57]. In spite of this discrepancy, the developed 2D model is still sufficient to capture the main feature of the observed electroosmotic flow patterns in our experiments, which will be presented in Ssection 4. We are currently developing a 3D model for this problem in order that realistic h values can be used in the simulation.

3 Results and discussion

Figure 3 shows the comparison of the experimentally obtained pathlines of 590 nm particles (bottom) and numerically predicted streamlines (top) of electroosmotic flow through the microchannel constriction under various DC-biased AC voltages. A video clip exhibiting the flow pattern changes during this variation is available in the Supporting Information. The total RMS magnitude of the applied DC and AC voltages was fixed at 600 V, yielding an average electric field of about 600 V/cm over the channel length. The frequency of the AC voltages was fixed at 1 kHz. We did not observe noticeable changes in the flow pattern

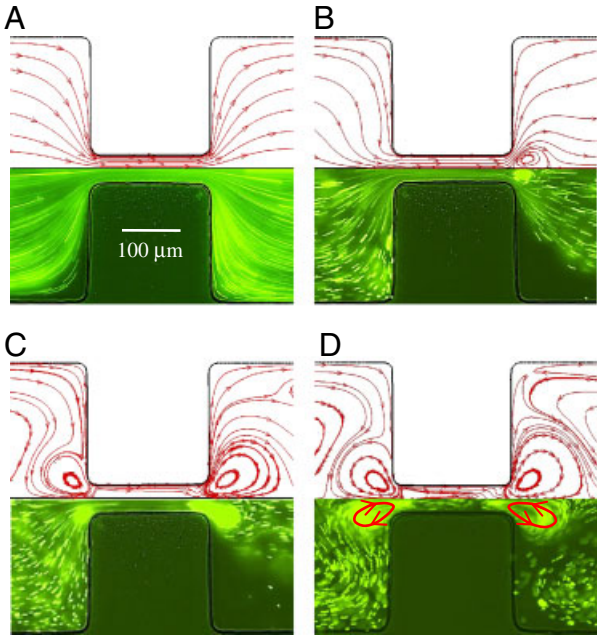

Figure 3. Comparison of simulation (top) and experimental (bottom) results of electroosmotic flow patterns in the microchannel constriction region under various DC-biased AC (fixed at 1 kHz) voltages: (A) 600 V DC, (B) 100 V DC/500 V AC, (C) 50 V DC/550 V AC, and (D) 20 V DC/580 V AC. The average electric field is about 600 V/cm over the channel length. The Joule heating-induced electrothermal flow circulations were observed to start occurring at the downstream end of the constriction under 100 V DC/500 V AC, see panel (B). The flow direction is from left to right in all cases. The arrowed loops in the experimental image of (D) indicate the directions of the electrothermal flow circulations.

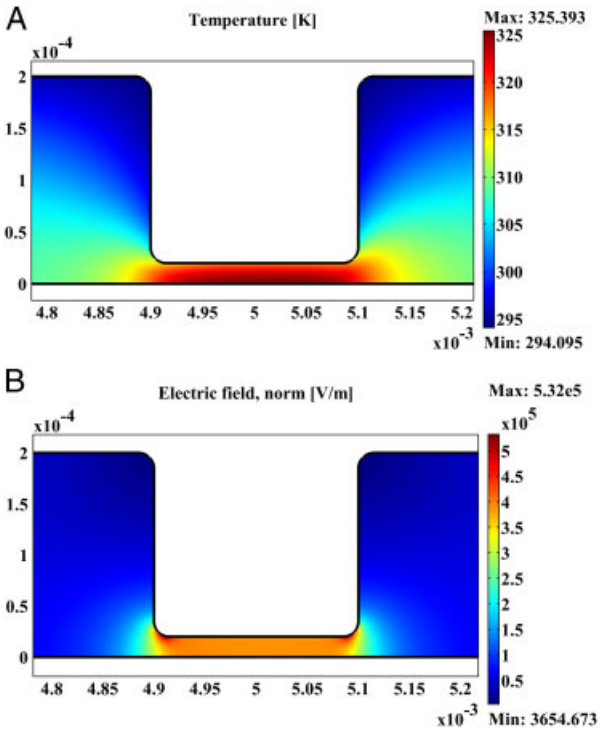

Figure 4. Illustration of the contours of fluid temperature (A) and electric field (B) in the microchannel constriction. The applied voltages are 100 DC and 500 V AC. The fluid reaches a high temperature within the constriction due to the locally amplified electric field, which is shifted slightly downstream due to electroosmotic flow. The flow direction is from left to right.

when the AC frequency was varied from 500 Hz to 10 kHz (the maximum frequency that our amplifier actually allows is <15 kHz). At frequencies lower than 200 Hz, the AC electrophoretic motion of particles was observed to blur the particles, which significantly affects the flow visualization. In addition, we noticed that the flow patterns in all cases presented below formed quickly after the voltage was supplied and appeared to achieve steady state within seconds. We are currently revising the experimental technique and numerical model in order to elucidate the transient development of electroosmotic flow in iDEP devices.

Under a 600 V DC voltage, there are no apparent disturbances to both the observed pathlines (bottom) and the predicted streamlines (top) in Fig. 3A as compared with the previously reported electroosmotic flow profiles in the presence of Joule heating [50, 55, 56]. However, when the DC voltage was decreased to 100 V and a 500 V AC voltage was applied to maintain the total magnitude, a pair of small counter-rotating circulations was observed to occur at the downstream end of the constriction in Fig. 3B. This phenomenon, as also predicted by our numerical modeling, indicates that the electrothermal flow induced in the constriction starts to become comparable to the reduced electroosmotic flow under a lowered DC voltage. The electrothermal fluid circulations appear to obstruct the electroosmotic flow in the channel center while enhancing it near the corners of the constriction. It is also noticed that the fluorescent particles cover a narrower region at the downstream side of the constriction than at the upstream side in the bottom image of Fig. 3B. This is believed to be a consequence of the constriction-induced dielectrophoretic focusing effect on 590 nm particles as we have demonstrated previously [25].

Similar to those previously studied in eDEP [34–47], electrothermal flows in iDEP devices also arise from the action of the electric field (both DC and AC) on fluid inhomogeneities (predominantly electrical properties including conductivity and permittivity) formed in the constriction region due to Joule heating-induced temperature gradients. Figure 4 shows the numerically predicted temperature and electric field contours in the constriction region at 100 V DC/500 V AC. As expected, the fluid temperature within the constriction is much higher than that outside it because the electric field is locally amplified by the constriction. Moreover, the axial temperature distribution is not exactly symmetric about the constriction, and actually shifts slightly

downstream due to the electroosmotic fluid advection, i.e. the convective term on the left-hand side of Eq. (5). This effect is more pronounced in the 500 V DC case, and is consistent with the temperature distribution in capillary or microchip-based electrophoresis, where the Joule heating-caused high temperature plateau in the main body of the capillary or microchannel shifts toward the outlet reservoir due to electroosmotic effect [55, 56].

Further decreasing the DC voltage to 50 V while increasing the AC voltage to 550 V, we observed electrothermal fluid circulations at both the downstream and the upstream ends of the channel constriction as demonstrated in Fig. 3C. However, the downstream circulations appeared to be larger in size than the upstream pair, which is also reasonably captured in our numerical modeling. Moreover, the upstream circulations were noticed to rotate in the mirror direction of the downstream ones. That is to say, the electrothermal body force ($\mathbf{f}_e$) tends to slow down the incoming fluid near the corners at the upstream end of the constriction, and then pull it to the channel center where the local electroosmotic fluid flow is enhanced by the electrothermal flow. As we continued decreasing the DC voltage to 20 V while increasing the AC voltage to 580 V, all circulations were observed to grow even larger in size, and the electrothermal flow seemed to dominate the electroosmotic flow in the constriction region. However, the upstream circulations are still a little smaller than the downstream ones due to the electroosmotic flow, which agrees qualitatively with the numerical modeling as demonstrated in Fig. 3D. It is noted that similar fluid circulations have been predicted numerically by Hawkins and Kirby [49] in a recent paper, where the electrothermal body force was considered for the first and the only time in studying Joule heating effects on electrokinetic transport in iDEP devices.

Using our previously developed model [20, 25], we estimated the potential influence of DEP on the trajectories of the 590 nm tracing particles in the above experiment. It was found that the induced dielectrophoretic velocity was on the order of 50 μm/s in the fluid circulation regions, and could reach 150 μm/s if the particle was within 2 μm distance from the corners of the constriction. Accordingly, the predicted electroosmotic fluid velocity varied approximately from 300 to 450 μm/s for the 20 V DC/580 V AC case, at which the electroosmotic flow was the weakest among the four cases shown in Fig. 3. We also attempted to track the particle rotation speed within the circulations, but were limited in our ability to do so by the strong fluid circulations. The minimum particle rotation speed that could be measured by our equipment was 1000 μm/s. Therefore, the Joule heating-induced electrothermal flow should dominate the particle motion in the 20 V DC/580 V AC case. For other cases in Fig. 3 with higher DC voltages, the electroosmotic flow itself should be large enough to dominate the particle motion. As a result, the observed trajectories of tracing particles are not significantly affected by the induced DEP, and can be used to compare with the numerically predicted fluid streamlines.

Under a 600 V pure AC voltage, there is no net electroosmotic flow in the microchannel. Therefore, the electrothermal fluid circulations should become symmetric about the constriction, which is clearly demonstrated in both the experiment (left plot) and the simulation (right plot, the background shows the fluid velocity contour and the lines represent fluid streamlines) in Fig. 5C. The same figure also shows the electrothermal flow patterns under 200 V (A), 400 V (B), and 800 V (D) pure AC voltages. In Fig. 5A fluid circulations are barely seen because the applied 200 V/cm electric field is too low to cause sufficient temperature gradients for electrothermal flows. As a matter of fact, the largest rise in fluid temperature under 200 V AC is <5 K at the center of the constriction as shown in Fig. 6. Increasing the AC voltage rapidly elevates the fluid temperature as Joule heating is proportional to the electric field squared, which is illustrated by the axial fluid temperature profiles along the channel centerline in Fig. 6. Consequently, increasing the AC voltage should dramatically enhance the electrothermal flow in the constriction region as the electrothermal force, ($\mathbf{f}_e$) in Eq. (9), scales with the fourth power of electric field. This is borne out by our experimental and simulation results in Fig. 5. It is important to note that the

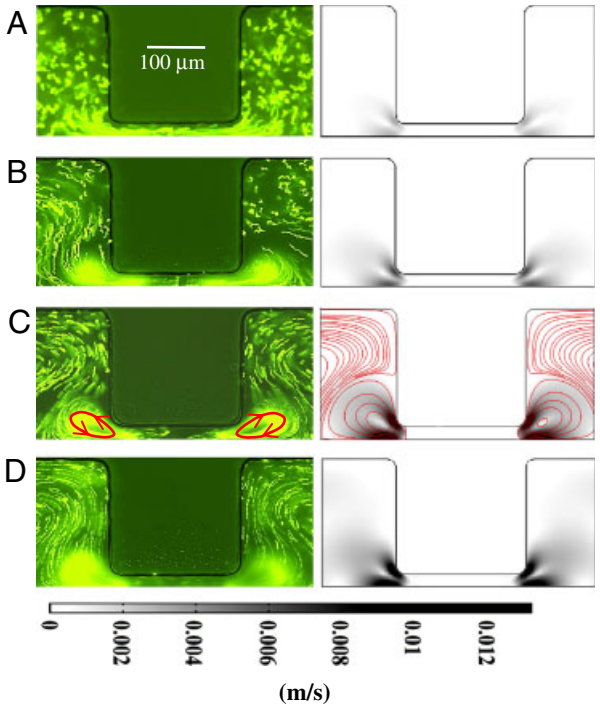

Figure 5. Comparison of simulation (right column, background shows the contour of fluid velocity) and experimental (left column) results of electroosmotic flow in the microchannel constriction region under various pure AC voltages (fixed at 1 kHz): (A) 200 V, (B) 400 V, (C) 600 V, and (D) 800 V. The simulation result in panel (C) also includes the fluid streamlines, whose directions are shown in Fig. 3. There is no net flow in the main channel. The arrowed loops in the experimental image of (C) indicate the directions of the electrothermal flow circulations.

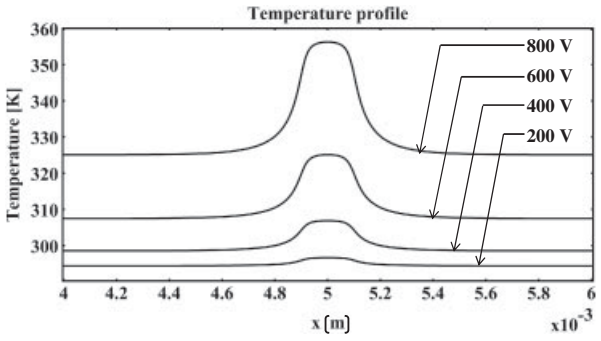

Figure 6. Comparison of the axial fluid temperature profiles along the centerline of the constriction microchannel under pure AC voltages ranging from 200 to 800 V. All profiles are symmetric about the constriction as there is no net electroosmotic flow in the channel.

results presented here are only valid for low-frequency AC electric fields and high-conductivity solutions.

4 Concluding remarks

We have performed a combined experimental and numerical study of Joule heating effects on electroosmotic flow in a typical iDEP device, i.e. a constriction microchannel. Fluid circulations were observed around the constriction for the first time using small fluorescent tracing particles. They are formed through a mechanism identical to the traditional AC electrothermal flow in eDEP devices, which, as verified by our numerical modeling, is attributed to the interaction between the applied electric field and the fluid inhomogeneities in the constriction region due to Joule heating-induced temperature gradients. Through both experimentation and simulation, we have examined how the DC (in DC-biased AC fields) and AC (in pure AC fields) voltages may alter the electroosmotic flow pattern in the constriction microchannel. It is found that the electrothermal fluid circulations grow in size and speed dramatically with the increasing AC voltage in both cases. Such Joule heating-induced electrothermal flow circulations should be taken into account in the design and operation of iDEP devices, especially when highly conductive solutions and/or large electric fields must be employed. They may potentially be harnessed to enhance microfluidic mixing and immunoassay for lab-on-a-chip applications. In future work we plan to make the fluid velocity and temperature measurements using micro particle image velocimetry (μPIV) technique [39] and the rhodamine B-based thermometry techniques [58], respectively. The obtained experimental results will then be compared quantitatively with the predictions of a 3D model that is currently under development in our lab.

This work was supported by NSF under grant CBET-0853873 and by Clemson University through a start-up package (X. X.). The support from the Knowledge Innovation Program of CAS (KJCX2-YW-H18) (G. H.) is also gratefully appreciated.

The authors have declared no conflict of interest.

5 Appendix

This appendix presents the modifications to the field equations in order to handle DC-biased AC electric fields in COMSOL. The electric potential equation, i.e. Eq. (4), is modified as

$$\nabla \cdot (\sigma \nabla \phi_{DC}) = 0 \tag{A1}$$

where ϕ_{DC} is the applied DC voltage. The energy equation, i.e. Eq. (5), is modified as

$$\rho Cp(\mathbf{u} \cdot \nabla T) = \nabla \cdot (k \nabla T) + (1+\lambda^2)\sigma \mathbf{E}_{DC}^2 \tag{A2}$$

where $\mathbf{E}_{DC} = -\nabla \phi_{DC}$ is the DC electric field, and λ is the ratio that relates the RMS value of the AC field to the magnitude of the DC field. Accordingly, the electrothermal body force, ($\mathbf{f}_e$) in Eq. (9), is modified as

$$\langle \mathbf{f}_e \rangle = (1+\lambda^2)[(\varepsilon \nabla \cdot \mathbf{E}_{DC} + \alpha \varepsilon_0 \mathbf{E}_{DC} \cdot \nabla T)\mathbf{E}_{DC} - 0.5\alpha \varepsilon_0 \mathbf{E}_{DC}^2 \nabla T] \tag{A3}$$

6 References

[1] Lapizco-Encinas, B. H., Rito-Palmomares, M., *Electrophoresis* 2007, *28*, 4521–4538.

[2] Hawkins, B. G., Gleghorn, J. P., Kirby, B. J., in: Zahn, J. D. (Ed.). *Methods in Bioengineering: Biomicrofabrication and Biomicrofluidics*, Artech House, Norwood, MA, 2009, pp. 133–181.

[3] Pethig, R., *Biomicrofluidics* 2010, *4*, 022811.

[4] Pohl, H. A., *Dielectrophoresis: The Behavior of Neutral Matter in Non-uniform Electric Fields*, Cambridge University Press, Cambridge 1978.

[5] Gascoyne, P. R. C., Vykoukal, J., *Electrophoresis* 2002, *23*, 1973–1983.

[6] Hughes, M. P., *Electrophoresis* 2002, *23*, 2569–2582.

[7] Chou, C. F., Zenhausern, F., *IEEE Eng. Med. Biology Mag.* 2003, *22*, 62–67.

[8] Cummings, E. B., *IEEE Eng. Med. Biology Mag.* 2003, *22*, 75–84.

[9] Srivastava, S. K., Gencoglu, A., Minerick, A. R., *Anal. Bioanal. Chem* 2010, *399*, 301–321.

[10] Choi, S., Park, J. K, *Lab Chip* 2005, *5*, 1161–1167.

[11] Kralj, J. G., Lis, M. T. W., Schmidt, M. A., Jensen, K. F., *Anal. Chem.* 2006, *78*, 5019–5025.

[12] Kim, U., Shu, C. W., Dane, K. Y., Daugherty, P. S., Wang, J. Y. J., Soh, H. T., *Proc. Natl. Acad. Sci.* 2007, *104*, 20708–20712.

[13] Vahey, M. D., Voldman, J., *Anal. Chem.* 2008, *80*, 3135–3143.

[14] Han, K. H., Frazier, A. B., *Lab Chip* 2008, *8*, 1079–1086.

[15] Wang, L., Lu, J., Marchenko, S. A., Monuki, E. S., Flanagan, L. A., Lee, A. P., *Electrophoresis* 2009, *30*, 782–791.

[16] Khoshmanesh, K., Zhang, C., Tovar-Lopez, F. J., Nahavandi, S., Nahavandi, S., Baratchi, S., Kalantar-Zadeh, K., Mitchell, A., *Electrophoresis* 2009, *30*, 3707–3717.

[17] Lewpiriyawong, N., Yang, C., Lam, Y. C., *Electrophoresis* 2010, *31*, 2622–2631.

[18] Lapizco Encinas, B. H., Simmons, B. A., Cummings, E. B., Fintschenko, Y., *Electrophoresis* 2004, *25*, 1695–1704.

[19] Barrett, L. M., Skulan, A. J., Singh, A. K., Cummings, E. B., Fiechtner, G. J., *Anal. Chem.* 2005, *77*, 6798–6804.

[20] Kang, K., Kang, Y., Xuan, X., Li, D., *Electrophoresis* 2006, *27*, 694–702.

[21] Pysher, M. D., Hayes, M. A., *Anal. Chem.* 2007, *79*, 4552–4557.

[22] Hawkins, B. G., Smith, A. E., Syed, Y. A., Kirby, B. J., *Anal. Chem.* 2007, *79*, 7291–7300.

[23] Lewpiriyawong, N., Yang, C., Lam, Y. C., *Biomicrofluidics* 2008, *2*, 034105.

[24] Ozuna-Chacón, S., Lapizco-Encinas, B. H., Rito-Palomares, M., Martínez-Chapa, S. O., Reyes-Betanzo, C., *Electrophoresis* 2008, *29*, 3115–3122.

[25] Zhu, J., Xuan, X., *Electrophoresis* 2009, *30*, 2668–2675.

[26] Zhu, J., Tzeng, T. J., Xuan, X., *Electrophoresis* 2010, *31*, 1382–1388.

[27] Baylon-Cardiel, J. L., Jesus-Perez, N. M., Chavez-Santoscoy, A. V., Lapizco-Encinas, B. H., *Lab Chip* 2010, *10*, 3235–3242.

[28] Voldman, J., *Annu. Rev. Biomed. Eng.* 2006, *8*, 425–454.

[29] Kang, Y. J., Li, D. Q., Kalams, S. A., Eid, J. E., *Biomed. Microdev.* 2008, *10*, 243–249.

[30] Gaš, B., Stedry, M., Kenndler, E., *Electrophoresis* 1997, *18*, 2123-2133.

[31] Xuan, X., *Electrophoresis* 2008, *29*, 33–43.

[32] Cetin, B., Li, D., *Electrophoresis* 2008, *29*, 994–1005.

[33] Evenhuis, C. J., Haddad, P. R., *Electrophoresis* 2009, *30*, 897–909.

[34] Muller, T., Gerardino, A., Schnelle, T. H., Shirley, S. G., Bordoni, F., De Gasperis, G., Leoni, R., Fuhr, G., *J. Phys. D* 1996, *29*, 340–349.

[35] Ramos, A., Morgan, H., Green, N. G., Castellanos, A., *J. Phys. D* 1998, *31*, 2338–2353.

[36] Green, N. G., Ramos, A., Gonzalez, A., Castellanos, A., Morgan, H., *J. Electrost.* 2001, *53*, 71–87.

[37] Castellanos, A., Ramos, A., Gonzalez, A., Green, N. G., Morgan, H., *J. Phys. D* 2003, *36*, 2584–2597.

[38] Perch-Nielsen, I. R., Green, N. G., Wolff, A., *J. Phys. D* 2004, *37*, 2323–2330.

[39] Wang, D., Sigurdson, M., Meinhart, C. D., *Exp. Fluid.* 2005, *38*, 1–10.

[40] Gonzalez, A., Ramos, A., Morgan, H., Green, N. G., Castellanos, A., *J. Fluid Mech.* 2006, *564*, 415–433.

[41] Burg, B. R., Bianco, V., Schneider, J., Poulikakos, D., *J. Appl. Phys.* 2010, *107*, 124308.

[42] Lee, H., Yun, S., Ko, S. H., Kang, K. H., *Biomicrofluidics* 2009, *3*, 044113.

[43] Garcia-Sanchez, P., Ramos, A., Mugele, F., *Phys. Rev. E* 2010, *81*, 015303.

[44] Ng, W. Y., Goh, S., Lam, Y. C., Yang, C., Rodriguez, I., *Lab Chip* 2009, *9*, 802–809.

[45] Feldman, H. C., Sigurdson, M., Meinhart, C. D., *Lab Chip* 2007, *7*, 1553–1559.

[46] Wu, J., Lian, M., Yang, K., *Appl. Phys. Lett.* 2007, *90*, 234103.

[47] Gagnon, Z. R., Chang, H. C., *Appl. Phys. Lett.* 2009, *94*, 024101.

[48] Sabounchi, P., Huber, D. W., Kanouff, M. P., Harris, A. E., Simmons, B. A., *Twelfth International Conferences on Miniaturized Systems for Chemistry and Life Sciences*, pp. 50–52, October 12–16, San Diego, CA, USA.

[49] Hawkins, B. J., Kirby, B. J., *Electrophoresis* 2010, *31*, 3622–3633.

[50] Erickson, D., Sinton, D., Li, D., *Lab Chip* 2003, *3*, 141–149.

[51] Melcher, J. R., Taylor, G. I., *Annu. Rev. Fluid. Mech.* 1969, *1*, 111–146.

[52] Kirby, B. J., *Micro- and Nanoscale Fluid Mechanics: Transport in Microfluidic Devices*, Cambridge University Press, Cambridge 2010.

[53] Xuan, X., Sinton, D., Li, D., *Int. J. Heat Mass Trans.* 2004, *47*, 3145–3157.

[54] Lide, D. R., CRC Handbook of Chemistry and Physics, 90 Edn, CRC Press, Boca Raton, FL 2009.

[55] Xuan, X., Xu, B., Sinton, D., Li, D., *Lab Chip* 2004, *4*, 230–236.

[56] Tang, G., Yang, C., *Electrophoresis* 2006, *27*, 628–639.

[57] Kates, B., Ren, C. L., *Electrophoresis* 2006, *27*, 1967–1976.

[58] Ross, D., Gaitan, M., Locascio, L. E., *Anal. Chem.* 2001, *73*, 4117–4123.

